CHEMISTRY

# Hypergolic zeolitic imidazolate frameworks (ZIFs) as next-generation solid fuels: Unlocking the latent energetic behavior of ZIFs

H. M. Titi[1], J. M. Marrett[1], G. Dayaker[1], M. Arhangelskis[1], C. Mottillo[1], A. J. Morris[2], G. P. Rachiero[1], T. Friščić[1]*, R. D. Rogers[1,3]*



**Hypergolic materials, capable of spontaneous ignition upon contact with an external oxidizer, are of critical importance as fuels and propellants in aerospace applications (e.g., rockets and spacecraft). Currently used hypergolic fuels are highly energetic, toxic, and carcinogenic hydrazine derivatives, inspiring the search for cleaner and safer hypergols. Here, we demonstrate the first strategy to design hypergolic behavior within a metal-organic framework (MOF) platform, by using simple "trigger" functionalities to unlock the latent and generally not recognized energetic properties of zeolitic imidazolate frameworks, a popular class of MOFs. The herein presented six hypergolic MOFs, based on zinc, cobalt, and cadmium, illustrate a uniquely modular platform to develop hypergols free of highly energetic or carcinogenic components, in which varying the metal and linker components enables the modulation of ignition and combustion properties, resulting in excellent hypergolic response evident by ultrashort ignition delays as low as 2 ms.**

## INTRODUCTION

Energetic materials (*1*–*4*), i.e., controllable chemical energy storage systems, are central for a number of civilian and military applications, including explosives, propellants, and pyrotechnics. Current research in this area is aimed toward materials with specific requirements, such as high energy density, improved thermal stability, low cost, and environmental acceptability (*5*–*8*). An important class of energetic materials is hypergolic materials, fuels (*9*, *10*) that ignite upon contact with an external oxidizer. Hypergolic compounds are a necessary component of spacecraft and launcher propellant systems (*11*), which require materials with a low ignition delay (ID), defined as the time between ignition and the first contact of the fuel with the oxidizer. The most popular hypergolic components of bipropellant systems today are based on toxic and highly carcinogenic hydrazine and its derivatives (*12*, *13*), raising concerns of environmental damage. As an example, the annual release of carcinogenic propellants in the atmosphere is estimated at 12,000 tons, inspiring the search for safer hypergolic fuels (*14*–*16*).

Metal-organic frameworks (MOFs) are advanced materials of principal importance in gas separation, storage, and catalysis (*17*, *18*) but have also been explored as energetic materials (*19*–*21*). In principle, MOFs should offer a highly modular platform (*22*) for developing solid (*4*) hypergolic ignition and fuel systems, where the ignition and combustion properties of the solid fuel can be fine-tuned by variation of both organic and inorganic components of the MOF. However, exploration of MOFs and coordination polymers as energetic materials has so far focused only on properties relevant to explosives or pyrotechnical materials, such as thermal and shock sensitivity (*19*, *23*). Hypergolicity, which is a critical property of a potential fuel or propellant, has not been investigated in context of MOFs or coordination polymers in general.

We now present a strategy to induce hypergolic behavior in MOFs by incorporating an acetylene or vinyl substituent as a trigger of hypergolicity in a zeolitic imidazolate framework (ZIF; Fig. 1A) (*24*). Whereas ZIFs are generally not considered energetic materials and exhibit high thermal stability (*24*, *25*), we noted a potential structural and electronic similarity between imidazole linkers in a ZIF, flanked on both nitrogen sites by cationic nodes, and energetic imidazolium cations used in energetic ionic liquids, similarly flanked by alkyl substituents (Fig. 1B). We hypothesized that the azolate linkers in a ZIF could exhibit latent energetic properties, which might be unlocked by introducing triggers of hypergolic behavior, such as vinyl or acetylene functionalities (*15*).

## RESULTS

Using imidazole ligands substituted in the 2-position by acetylene (H**AIm**) and vinyl (H**VIm**) groups (Fig. 1B and figs. S1 and S2), we targeted ZIFs based on $Zn^{2+}$, $Co^{2+}$, and $Cd^{2+}$ cations that not only are popular in ZIF synthesis but also provide an opportunity to systematically vary size and electronic properties of framework nodes. All six ZIFs were readily accessible by previously described ion- and liquid-assisted grinding (ILAG) mechanochemical methods for ZIF synthesis (*26*), i.e., by ball-milling equimolar amounts of a metal source [ZnO, $CoCO_3$, $Cd(OH)_2$, or CdO] and a substituted imidazole, in the presence of a liquid additive and a salt catalyst. In all six cases, powder x-ray diffraction (PXRD) revealed quantitative formation of products isostructural to ZIF-8 (CSD OFERUN02) (*27*), the popular sodalite (SOD) topology ZIF based on 2-methylimidazole (fig. S3). The structure of guest-free SOD-Zn(**VIm**)$_2$ was recently reported (CSD GAZBOB) (*28*), which facilitated the creation of a preliminary structural model for each framework, and the final structures were obtained by Rietveld refinement of PXRD data on MOF samples that were washed with methanol and evacuated (Fig. 2 and table S1). Composition of each MOF was verified by thermogravimetric analysis (TGA; figs. S4 and S5) in air, and the absence of starting material was confirmed by Fourier transform infrared attenuated total reflectance (FTIR-ATR) spectroscopy and solid-state nuclear magnetic resonance (NMR) spectroscopy

[1]Department of Chemistry, McGill University, Montreal, QC H3A 0B8, Canada. [2]School of Metallurgy and Materials, University of Birmingham, Edgbaston, Birmingham B15 2TT, UK. [3]525 Solutions Inc., P.O. Box 2206, Tuscaloosa, AL 35403, USA.
*Corresponding author. Email: tomislav.friscic@mcgill.ca (T.F.); robin.rogers@525solutions.com (R.D.R.)

(figs. S6 and S7). Combined TGA and differential scanning calorimetry (DSC) revealed high thermal stability in air for all MOFs, with exothermic degradation above 200°C. The materials were also not sensitive to impact, with no detonation taking place even upon impacts of 50 J.

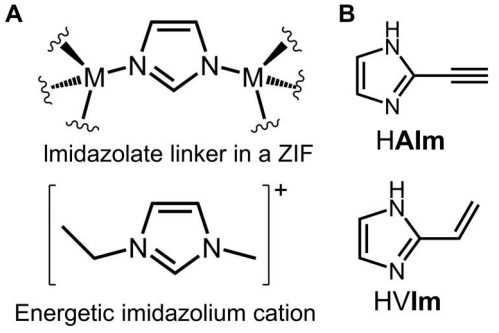


**Fig. 1. The design and molecules used herein for the development of hypergolic ZIFs.** (**A**) Similarity between the organic linker in a ZIF (top) and a typical energetic imidazolium cation (bottom). (B) The ligands H**AIm** and H**VIm** used in the development of hypergolic ZIFs.

The stability to impact was confirmed by PXRD analysis of the materials after impact tests (fig. S8).

Hypergolic properties were evaluated by measuring the ID for each material using a standard drop test (*29*), in which a single 10-μl drop of a liquid oxidizer was released from a fixed height of 5.0 cm, using a 100-μl Hamilton microsyringe, into a 4.5-cm-high glass vial, containing 5.0 mg of the solid fuel MOF or pure ligand, placed in the center. White fuming nitric acid (WFNA, 98% $HNO_3$) and less potent red fuming nitric acid (RFNA, more than 90% $HNO_3$), which are conventionally used in propellant systems, were used as oxidizers (*15*, *30*). Each drop test was done three times and recorded using a monochrome Redlake MotionPro Y4 high-speed camera operating at 1000 frames/s. The tests were done on Zn(**AIm**)$_2$, Co(**AIm**)$_2$, Cd(**AIm**)$_2$, Zn(**VIm**)$_2$, Co(**VIm**)$_2$, and Cd(**VIm**)$_2$, as well as on H**AIm**, H**VIm** (Fig. 2), and two ZIFs containing saturated hydrocarbon groups that were not expected to exhibit hypergolicity: ZIF-8 due to isostructurality to herein prepared ZIFs and open RHO topology zinc 2-ethylimidazolate [RHO-Zn(**EtIm**)$_2$] as a saturated analog of Zn(**AIm**)$_2$ and Zn(**VIm**)$_2$.

As anticipated, drop tests with WFNA and RFNA (Fig. 2, Table 1, and fig. S9) revealed no ignition for ZIF-8 and RHO-Zn(**EtIm**)$_2$. In contrast, Zn(**AIm**)$_2$, Co(**AIm**)$_2$, and Cd(**AIm**)$_2$ exhibited high hypergolic

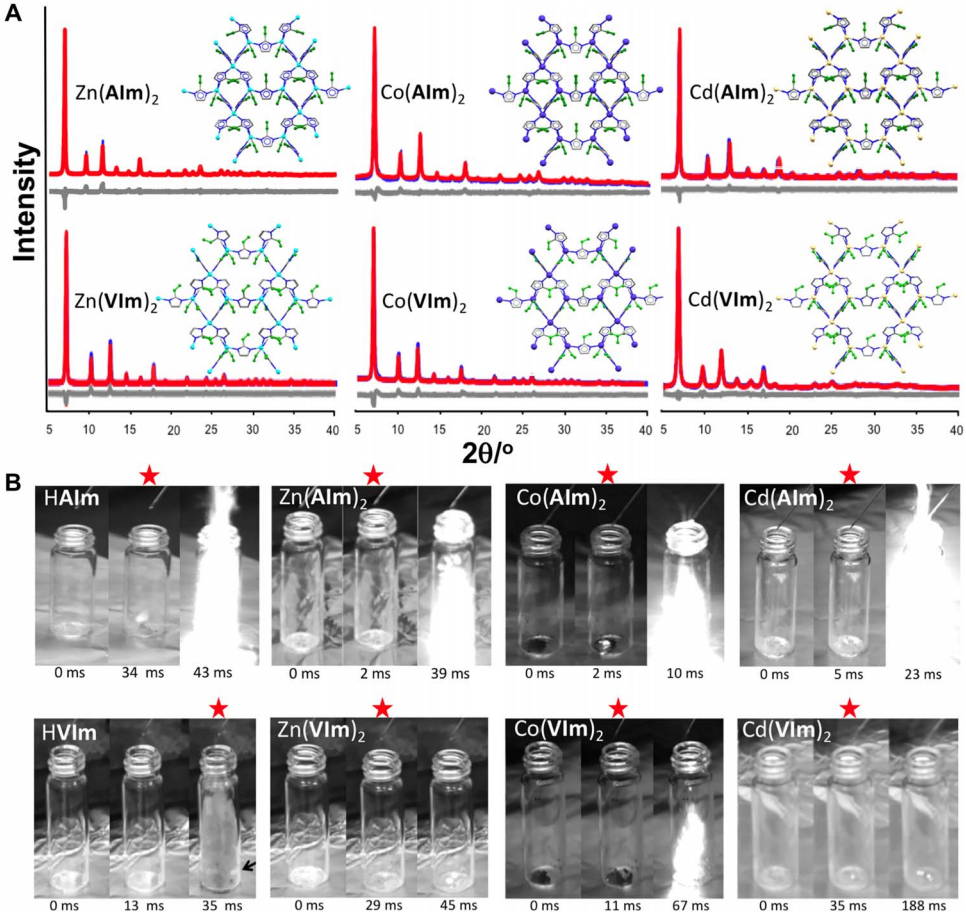


**Fig. 2. Structural analysis and hypergolic properties of hypergolic ZIFs.** (A) Final Rietveld fits for Zn(**AIm**)$_2$, Co(**AIm**)$_2$, and Cd(**AIm**)$_2$ (top row) and for Zn(**VIm**)$_2$, Co(**VIm**)$_2$, and Cd(**VIm**)$_2$ (bottom row). (**B**) Examples of hypergolicity drop tests for H**AIm**, Zn(**AIm**)$_2$, Co(**AIm**)$_2$, and Cd(**AIm**)$_2$ (top row) and for H**VIm**, Zn(**VIm**)$_2$, Co(**VIm**)$_2$, and Cd(**VIm**)$_2$ (bottom row). The moment of ignition for each experiment is indicated by a red star. Each drop test was conducted in triplicate (see Table 1). Photo credit: Hatem M. Titi, McGill University.

**Table 1. Hypergolic properties of herein explored ZIFs and corresponding ligands in drop tests using WFNA and RFNA as oxidizers.** Each test was conducted in triplicate.

| Fuel | Drop test with WFNA | | | | Drop test with RFNA | | | |
|---|---|---|---|---|---|---|---|---|
| | ID (ms) | Flame duration (ms) | Flame height* (cm) | Flame color | ID (ms) | Flame duration (ms) | Flame height* (cm) | Flame color |
| Zn(**AIm**)$_2$ | 2(1), 4(1)† | >600 | 4 | Red, blue | 12(2) | <150 | 4 | Red, blue |
| Co(**AIm**)$_2$ | 2(1), 2(1)† | >200 | 4 | Orange | 7(2), 10(2)† | >200 | 5 | Orange |
| Cd(**AIm**)$_2$ | 5(1), 3(2)† | >200 | 6 | Yellow | 30(2) | <150 | 4 | Orange |
| Zn(**VIm**)$_2$ | 29(1) | Sparks | Sparks | Red | –‡ | – | – | Smoke |
| Co(**VIm**)$_2$ | 11(5) | >200 | 2 | Orange | 164§ | Sparks | – | Orange |
| Cd(**VIm**)$_2$ | 35(1) | Sparks | Sparks | Yellow | –‡ | – | – | Smoke |
| ZIF-8 | –‡ | – | – | – | –‡ | – | – | – |
| Zn(**EtIm**)$_2$‖ | –‡ | – | – | – | –‡ | – | – | – |
| H**AIm** | 34(4) | >100 | 7 | Red | –‡ | – | – | Smoke |
| H**VIm** | 34(2) | Sparks | Sparks | Red | –‡ | – | – | Smoke |

*Approximate values. †Sample made from solution. ‡No ignition. §Ignited in only one of three tests. ‖RHO topology framework.

behavior with WFNA, with ultrashort IDs (below 5 ms) (*15*) and appearance of a flame with 4 to 6 cm in height. Similar results were obtained for samples made from solution (Table 1), indicating that method of preparation does not notably affect hypergolic behavior. The vinyl-substituted MOFs were also hypergolic with WFNA, with short IDs between 11 and 35 ms. For comparison, a target ID in the development of a functional hypergolic propellant is 50 ms or below (*16*). Consistent results were obtained using RFNA, where drop tests showed highly hypergolic behavior for Zn(**AIm**)$_2$, Co(**AIm**)$_2$, and Cd(**AIm**)$_2$ and weak hypergolicity for Co(**VIm**)$_2$. The drop tests confirm that incorporating vinyl or acetylene groups onto the ZIF scaffold promotes hypergolic behavior, previously not reported in ZIFs. The pure ligands H**AIm** and H**VIm** show poor (with WFNA) or no (with RFNA) hypergolic performance, which is improved upon ZIF formation.

The prepared MOFs are expected to be microporous, as already established for Zn(**VIm**)$_2$, with a reported surface area of 1091 $m^2/g$ (*28*). Nitrogen sorption experiments on Zn(**AIm**)$_2$, Co(**AIm**)$_2$, and Co(**VIm**)$_2$ materials after washing and evacuation revealed high Brunauer-Emmet-Teller (BET) surface areas of 1215, 1135, and 1210 $m^2/g$, respectively (fig. S10). To verify whether the microporous nature of the MOFs, notably, their ability to absorb the liquid oxidizer, could influence hypergolic behavior, we explored the ignition and combustion properties of the best-performing Zn(**AIm**)$_2$ and Co(**AIm**)$_2$ materials saturated with nitromethane, a guest molecule similar to $HNO_3$ in shape and size. The materials readily incorporated between approximately 14 and 17% by weight of nitromethane (fig. S11) but still exhibited ultrashort IDs of 5(3) and 3(1) ms with WFNA, respectively (fig. S12). These results indicate that the ability to include the oxidizer in the MOF is not critical for hypergolic response. A very short ID of 3 ms was also measured for Co(**AIm**)$_2$ saturated with *N*,*N*-dimethylformamide (DMF), demonstrating that the nature of the guest is also not critical for hypergolic performance.

Particularly notable is the comparison of hypergolic activity of H**AIm**, which exhibits an ID of 34(4) ms with WFNA and does not ignite at all with RFNA, to the corresponding ZIFs, which exhibited ID times as low as 2(1) ms (with WFNA) and 7(2) ms (with RFNA). These results show that the formation of coordination bonds in a ZIF can improve hypergolic behavior compared to the free ligand. This makes the design of hypergolic MOFs different from strategies for making energetic MOFs, where coordination bond formation leads to reduced thermal and impact sensitivity of an energetic ligand (*19*, *31*, *32*). The importance of ZIF formation for hypergolic behavior is evident from drop tests that were conducted on physical mixtures of pure ligands with ZnO or $CoCO_3$. Mixtures of H**AIm** with ZnO and $CoCO_3$ exhibited even poorer hypergolic behavior than the pure ligand, producing only sparks after delays of 46 to 117 ms (for ZnO) and 67 to 116 ms (for $CoCO_3$). Similarly, mixtures of H**VIm** and ZnO produced only sparks with delays in the range of 22 to 47 ms, whereas mixtures with $CoCO_3$ produced sparks only upon adding a second drop of oxidizer, after more than 1 s.

The isostructurality of all six hypergolic MOFs enables a systematic analysis of hypergolic behavior with respect to metal and linker choice. Overall, ZIFs derived from H**AIm** exhibited shorter IDs and more vigorous combustion compared to the ones derived from H**VIm** (Fig. 2 and Table 1), indicating that the acetylene group is more efficient in inducing hypergolic behavior. The zinc- and cobalt-based MOFs generally exhibited shorter IDs compared to cadmium ones, which agrees with a larger radius and poorer electron-withdrawing properties of $Cd^{2+}$. $Co^{2+}$ gave hypergolic properties comparable or superior to those of either zinc or cadmium frameworks: ID for Co(**AIm**)$_2$ is identical (with WFNA) or significantly shorter (with RFNA) compared to Zn(**AIm**)$_2$. Moreover, Co(**VIm**)$_2$ was the only vinyl-substituted ZIF that developed a flame with WFNA and the only vinyl-substituted MOF that was hypergolic with RFNA. As $Zn^{2+}$ and $Co^{2+}$ are of similar size, we tentatively relate the high hypergolicity of Co(**AIm**)$_2$ and Co(**VIm**)$_2$ to the open d-shell configuration of $Co^{2+}$ and, potentially, to the ability

of the metal node to undergo redox reactions. To better understand the effect of choice of metal node on reactivity of hypergolic MOFs, we used CASTEP (CAmbridge Serial Total Energy Package) periodic density functional theory (DFT) calculations to evaluate the bandgap for each material, accompanied by a density-of-states (DOS) analysis (fig. S13 and table S3). A reduction in the calculated bandgap has previously been related to an increase in the reactivity of energetic MOFs and coordination polymers (*33*, *34*). Our calculations indicate that a similar relationship might be valid for the reactivity of hypergolic MOFs, as the calculated bandgaps of vinyl- or acetylene-substituted MOFs decrease in the order of Cd > Zn > Co, i.e., in the same order that MOF hypergolicity increases. Whereas the exact mechanisms through which different metal nodes induce differences in MOF hypergolicity remains unknown, this agreement between bandgap calculations and experimentally measured IDs suggests that differences in hypergolicity of MOFs based on different metals should be related to their electronic structure.

Drop tests with WFNA were also performed on Zn(**AIm**)$_2$, Co(**AIm**)$_2$, and Cd(**AIm**)$_2$ made from solution (Table 1), again revealing ultrashort IDs below 5 ms. Hypergolic tests on Zn(**AIm**)$_2$, Co(**AIm**)$_2$, and Cd(**AIm**)$_2$ after 1 month of storage in a closed vial revealed a short ID of 4(1) ms for Zn(**AIm**)$_2$ but diminished activity for Co(**AIm**)$_2$ [ID of 54(5) ms] (fig. S14). Hypergolicity of Cd(**AIm**)$_2$ dropped significantly upon storage, producing only sparks in drop tests. The retention of hypergolic activity upon storage, evident for Zn(**AIm**)$_2$, is an important factor for applications in solid fuels.

To verify whether the observed hypergolic behavior is indeed the result of using trigger groups to unlock the suspected latent energetic behavior of ZIFs, we used CASTEP (*35*) periodic DFT calculations to evaluate the combustion energies ($\Delta E_c$) for reactions of hypergolic MOFs Zn(**AIm**)$_2$, Co(**AIm**)$_2$, Cd(**AIm**)$_2$, Zn(**VIm**)$_2$, Co(**VIm**)$_2$, and Cd(**VIm**)$_2$, as well as the nonhypergolic ZIF-8 with $O_2$ gas to produce solid ZnO, CdO, or $Co_3O_4$ along with $CO_2$, $N_2$, and $H_2O$ gas (equations given in table S2). The calculations were performed using the generalized gradient approximation–type Perdew-Burke-Ernzerhof (PBE) functional (*36*) combined with Grimme D2 (*37*) dispersion correction, and crystal structures of ZIFs were geometry-optimized with respect to atom coordinates and unit cell parameters, subject to space group symmetry constraints (fig. S15). The gravimetric ($E_g$) and volumetric ($E_V$) energy densities were computed from $\Delta E_c$, taking into account the calculated density of ZIFs. The accuracy of calculations was verified by comparing the herein calculated $\Delta E_c$ for ZIF-8 (−3916.0 kJ mol$^{-1}$) to the combustion enthalpy ($\Delta H_c$) that was also measured herein by bomb calorimetry (−4654.0 kJ mol$^{-1}$). The comparison shows that the calculated values are reasonably accurate and probably underestimate true values by ca. 15%.

All oxidation reactions were calculated to be highly exothermic, with $\Delta E_c$ ranging from −4700 to −4800 kJ mol$^{-1}$ (Table 2). The $\Delta E_c$ values of vinyl- and acetylene-substituted ZIFs were similar to that of ZIF-8, which confirms that acetylene and vinyl substituents act as triggers for hypergolic behavior, without notably increasing the energetic content of the ZIFs. The energetic content is significant, as the calculated $E_g$ and $E_V$ for all herein explored ZIFs, including ZIF-8, are actually comparable to popular explosives [e.g., trinitrotoluene (14.9 kJ g$^{-1}$)] (*38*) and hydrazine fuels (19.5 kJ g$^{-1}$ and 19.3 kJ cm$^{-3}$) (*39*).

**Table 2. Calculated combustion energy $\Delta E_c$, gravimetric ($E_g$) and volumetric ($E_V$) energy density, and crystallographic unit cell parameter (*a*) for ZIFs.**

| ZIF | $\Delta E_c$/kJ mol$^{-1}$ | $E_g$/kJ g$^{-1}$ | $E_V$/kJ cm$^{-3}$ | *a*/Å |
|---|---|---|---|---|
| Zn(**AIm**)$_2$ | −4783.8 | 19.3 | 19.3 | 17.045(1) |
| Co(**AIm**)$_2$ | −4760.0 | 19.7 | 19.5 | 16.960(2) |
| Cd(**AIm**)$_2$ | −4799.9 | 16.3 | 16.5 | 17.9721(9) |
| Zn(**VIm**)$_2$ | −4789.9 | 19.0 | 18.9 | 17.147(2)* |
| Co(**VIm**)$_2$ | −4767.6 | 19.5 | 18.4 | 17.296(1) |
| Cd(**VIm**)$_2$ | −4808.4 | 16.1 | 15.8 | 18.234(2) |
| ZIF-8 | −3916.0† | 17.2‡ | 15.9§ | 16.992(1)‖ |

*From CSD structure GAZBOB (*28*). †Measured enthalpy of combustion ($\Delta H_c$) is −4649.0 kJ mol$^{-1}$. ‡20.6 kJ g$^{-1}$ based on measured $\Delta H_c$. §18.9 kJ cm$^{-3}$ based on measured $\Delta H_c$. ‖CSD structure OFERUN02 (*27*).

## DISCUSSION

In summary, we described a strategy to induce hypergolic behavior in MOFs by using acetylene and vinyl substituents to unlock the latent energetic properties of electron-deficient linkers in a ZIF. This strategy also uses the formation of coordination bonds to enhance the hypergolic reactivity of the ligand, which is intrinsically different from approaches used to design other types of energetic (e.g., explosive and pyrotechnic) MOFs (*19*, *40*, *41*), where the formation of an extended structure often leads to ligand stabilization, in the form of reduced heat and shock sensitivity, sometimes accompanied by increased heat of detonation due to an energetic ligand being trapped in a nonpreferred conformation (*31*, *32*). The modularity of MOFs permits modification of the hypergolic properties (ID, flame color, and duration) of the fuel, including achieving ultrashort IDs, without changing its overall structure. Note that the acetylene or vinyl triggers induce hypergolicity without major changes to the overall energetic content of the ZIF structure. The ability to achieve and fine-tune hypergolic performance, combined with the absence of hydrazine-based carcinogens or explosive components, should make hypergolic MOFs promising candidates for safer, environmentally friendly propellants. We are currently investigating the use of other transition metals besides cobalt and zinc as nodes to facilitate the discovery of new MOF hypergols and understand the relationship between the choice of metal node and hypergolic behavior.

## MATERIALS AND METHODS

Solvents tetrahydrofuran, methanol, DMF, acetone, and chloroform were obtained from a PureSolv PS-400 solvent purification system. Thin-layer chromatography was performed on aluminum precoated silica gel plates from Merck, and developed plates were visualized by ultraviolet light (254 nm). Column chromatography was performed using flash chromatography with the indicated eluent on SiliaFlash P60, 40- to 63-μm silica gel. ZnO (Sigma-Aldrich), ammonium acetate (Sigma-Aldrich), ammonium sulfate (Sigma-Aldrich), CdO (Sigma-Aldrich), $Cd(NO_3)_2{\cdot}4H_2O$ (Macco), $CoCO_3$ (Alfa Aesar), and $Co(NO_3)_2{\cdot}6H_2O$ (Sigma-Aldrich) were used as received. Cadmium(II) hydroxide was synthesized from $Cd(NO_3)_2{\cdot}4H_2O$ by precipitation with NaOH, followed by washing with water and drying in air. Reactions under argon (synthesis of H**AIm**) were conducted in oven-dried glassware (120°C, minimum of 12 hours).

### NMR spectroscopy

Solution $^1$H NMR spectra (300 MHz) and $^{13}$C NMR spectra (75 MHz) were recorded on a Bruker AMX300 spectrometer. Chemical shifts were reported relative to dimethyl sulfoxide (DMSO)-$d_6$ [δ = 2.50 parts per million (ppm)] for $^1$H NMR spectra and DMSO-$d_6$ (δ = 39.5 ppm) for $^{13}$C NMR spectra. The $^1$H NMR spectra data were presented as follows: chemical shift, multiplicity (s, singlet; br., broad), and integration.

Solid-state cross-polarization magic angle spinning (CP-MAS) $^{13}$C NMR spectra were acquired on a Varian VNMRS 400 MHz NMR spectrometer operating at 100.53 MHz for $^{13}$C and at 399.77 MHz for $^1$H using a wide-bore 4-mm T3 double-resonance probe spinning at 14 kHz. Cross-polarization using RAMP CP (ramped-amplitude cross-polarization) for 5 ms at a radio frequency (rf) field of approximately 62 kHz on $^1$H was used. SPINAL-64 $^1$H decoupling was performed during acquisition using a 90-kHz rf field.

### FTIR-ATR spectroscopy

The FTIR-ATR spectra were obtained using a Bruker Vertex 70 FTIR spectrometer equipped with the Platinum ATR accessory.

### Mass spectrometry

Mass spectrometry on H**AIm** and H**VIm** was performed using an Exactive Plus Orbitrap mass spectrometer from Thermo Fisher Scientific.

### TGA and DSC

Simultaneous TGA and DSC were conducted on a TGA/DSC 1 (METTLER TOLEDO, Columbus, OH, USA), with samples (2 to 10 mg) placed in open 70-μl alumina crucibles. All measurements were done in a dynamic atmosphere of air, with a gas flow of 60 to 65 ml min$^{-1}$, and the samples were heated up to 700°C at a constant rate of 10°C min$^{-1}$.

### Powder x-ray diffraction

PXRD data were collected on a Bruker D2 PHASER diffractometer equipped with a LynxEye linear position sensitive detector (Bruker AXS, Madison, WI, USA), using Ni-filtered CuKα radiation. The PXRD pattern of Co(**AIm**)$_2$ was collected on a Bruker D8 Advance diffractometer equipped with a LynxEye-XE linear position sensitive detector (Bruker AXS, Madison, WI, USA) using Ni-filtered CuKα radiation.

Rietveld refinement (table S1) was performed using the software TOPAS Academic version 6 (Coelho Software). All ZIF structures were refined with a cubic *I*-43 *m* space group. Diffraction peak shapes were described by a pseudo-Voigt function, whereas the background was modeled with a Chebyshev polynomial function. The linker geometry was defined by a rigid body, which was given rotational and translational degrees of freedom, subject to the space group symmetry constraints. For the vinyl-substituted ligand, a flexible torsion angle allowing rotation of the vinyl group relative to the imidazole plane was defined. Last, a soft restraint was applied to the Metal–N bond (2.0 Å for Zn–N and Co–N bonds and 2.2 Å for Cd–N bond).

### Hypergolic testing

WFNA and RFNA are highly corrosive oxidizing agents and should be treated with care. In performing drop tests, the MOFs or corresponding solid ligands were exposed to one drop (10 μl volume) of WFNA or RFNA via a 100-μl Hamilton syringe (Hamilton, Reno, NV, USA). The liquid was dropped from a fixed height (5 cm) into a 4.5-cm vial containing approximately 5 mg of the particular material being tested. A Redlake MotionPro Y4 (Tallahassee, FL, USA) high-speed charge-coupled device camera was used to capture the event at 1000 frames/s. ID was considered to be the time between the contact of the oxidizing liquid with the solid material and the subsequent ignition and was measured by counting the frames between the two events. The test was repeated three times, the values for ID were averaged, and a standard deviation was calculated. For testing of the hypergolic behavior of MOFs containing included guests, ca. 50 mg of Zn(**AIm**)$_2$ or Co(**AIm**)$_2$ was stirred overnight in 1 ml of either nitromethane or DMF, filtered, and dried briefly in air.

### Bomb calorimetry

The bomb calorimetry measurement on ZIF-8 was carried out on the 6200 Isoperibol Calorimeter (Parr Instrument Company, Moline, IL, USA), which is a microprocessor-controlled, isoperibol oxygen bomb calorimeter.

### Impact sensitivity testing

Impact sensitivity testing was performed with a standard hammer drop test, using a 2.7-kg hardened steel weight that was released from a height of up to 2.1 m (corresponding to impact of ca. 50 J) onto an approximately 25-mg sample of Zn(**AIm**)$_2$, Zn(**VIm**)$_2$, Co(**AIm**)$_2$, or Co(**VIm**)$_2$. Each sample was placed between two hardened steel discs. No detonation or ignition was observed for any of the samples even at 50-J impact.

### Nitrogen sorption measurements

Nitrogen adsorption and desorption isotherm measurements were performed on a Micromeritics TriStar II instrument at a temperature of 77 K. Before measuring the nitrogen adsorption–desorption isotherms, the materials were activated by washing the samples with ethanol and chloroform and kept in vacuum oven overnight at 85°C. The calculated BET surface areas of Zn(**AIm**)$_2$, Co(**AIm**)$_2$, and Co(**VIm**)$_2$ were established to be 1215, 1135, and 1210 m$^2$/g, respectively.

### Computational methods

Periodic DFT calculations were performed using a plane wave DFT code CASTEP 16.11. The input files were prepared from experimental crystal structures using a program CIF2Cell (*42*). Structures were geometry-optimized with respect to atom coordinates and unit cell parameters, subject to the symmetry constraints of *I*-43 *m* space group. In case of vinyl-substituted ZIFs, the symmetry was lowered to *P*1 to resolve the disorder of the vinyl group (fig. S1).

Geometry optimization calculations were performed with PBE functional, and van der Waals interactions were modeled using Grimme D2 dispersion correction. The plane wave basis set was truncated at 750 eV, and norm-conserving pseudopotentials were used to modify the Coulomb potentials in the atom core regions. The Brillouin zone was sampled with a 0.03 Å$^{-1}$ Monkhorst-Pack k-point grid. The following convergence criteria were used: a maximum energy change of 10$^{-5}$ eV/atom, a maximum force on atom of 0.01 eV/Å, a maximum atom displacement of 0.001 Å, and a residual stress of 0.05 GPa.

We have optimized the structures of all herein prepared ZIFs. In addition, calculations were performed for the compounds involved in the combustion reaction (ZnO, $Co_3O_4$, CdO, $O_2$, $CO_2$, $N_2$, and $H_2O$). The gas-phase reaction components ($O_2$, $CO_2$, $N_2$, and $H_2O$) were modeled by placing a molecule in a cubic box of 30-Å length. This box size was found to be sufficient to make interactions between the periodic images negligibly small. The cell size was kept fixed, and the calculation was performed at the Γ point only to reflect the lack of periodicity in the

system. The reaction equations used to calculate combustion energies are given in table S2.

A DOS analysis was performed for ZIF structures in their optimized geometries. These calculations used the same functional, plane wave cutoff, and pseudopotentials as for geometry minimization. The electronic Brillouin zone, however, was sampled with a denser Monkhorst-Pack k-point grid of 0.015 $Å^{-1}$. The DOS plots were constructed with the program OptaDOS (fig. S13) (*43*, *44*). The DOS analysis was used to compute the bandgaps and correlate them with ZIF hypergolic performance.

## Synthetic methods

### *Synthesis of 2-substituted imidazoles*

Compound H**VIm** was synthesized following the previously reported procedure (*28*). Compound H**AIm** was synthesized on the basis of a modified procedure reported by Dirat and co-workers (*45*) (fig. S2). To a solution of aldehyde (0.336 g, 3.5 mmol) and dimethyl 1-diazo-2-oxopropylphosphonate (1.0 g, 5.25 mmol) in MeOH (15 ml) was added $K_2CO_3$ in one portion at 0°C under argon. The resulting yellow mixture was allowed to stir at room temperature for 12 hours. The reaction mixture was filtered through a Celite pad, and the solvent was concentrated under reduced pressure. The resulting crude mixture was diluted with 20 ml of water and extracted with EtOAc (2 × 30 ml), and the combined organic layers were washed with saturated $NaHSO_3$ (1 × 20 ml) and saturated NaCl (1 × 20 ml), dried over $MgSO_4$, and concentrated. Purification by flash chromatography on silica gel (methanol/dichloromethane: 1.5/98.5 to 2.5/97.5 v/v) afforded pure alkyne (0.138 g, 43%) as a white solid [melting point: 146.7 to 148.3; $R_f$: 0.5 (eluent: methanol/dichloromethane, 05:95 v/v); FTIR-ATR: 3273, 3141, 3112, 3015, 2122, 1568, 1420, 1299, 1106, 986, 899, 757, 700, 610, and 597 $cm^{-1}$ (fig. S7); $^1H$ NMR (300 MHz, DMSO-$d_6$; fig. S3): δ = 12.79 ppm (br. s, $^1H$), δ = 7.05 ppm (br. s, $^2H$), and δ = 4.30 ppm (s, $^1H$); $^{13}C$ NMR (75 MHz, DMSO-$d_6$; fig. S4): d = 128.4, 123.5, 80.4, and 75.3 ppm; high-resolution mass spectrometry (HRMS): calculated for $C_5H_5N_2$ $(M + H)^+$ 93.04472, found 93.04509 (fig. S7); solid-state CP-MAS $^{13}C$ NMR (100 MHz): 74.8, 80.6, 118.7, and 128.5 ppm (fig. S5)].

*Synthesis of SOD-Zn(AIm)$_2$ and SOD-Zn(MeIm)$_2$ (ZIF-8).*

**Mechanochemical synthesis:** These zinc-based ZIFs were synthesized using the ILAG methodology (*26*) by milling of 1 mmol of ZnO with an equivalent amount (2 mmol) of the imidazole ligand HAIm or HMeIm, in the presence of 0.12 mmol of ammonium acetate as the catalytic salt and 100 μl of ethanol as the liquid additive (absolute, kept over molecular sieves), in a 15-ml stainless steel milling jar using two stainless steel milling balls 7 mm in diameter (mass, 1.34 g each). The mixture was milled for 30 min at a frequency of 30 Hz in a (Retsch MM400 mixer mill). After the PXRD analysis, the product was stirred overnight with 15 ml of methanol, filtered, and evacuated under vacuum at 80°C. Solid-state CP-MAS $^{13}C$ NMR values (100 MHz) for Zn(AIm)$_2$ are as follows: 75.4, 125.5, and 135.7 ppm (fig. S7).

**Solution synthesis (SOD-Zn(AIm)$_2$**: A mixture of 2 mmol of H**AIm** and 2 mmol of triethylamine was added to 15 ml of DMF and stirred at room temperature. A solution of 1 mmol of zinc nitrate hexahydrate in 5 ml of DMF was added dropwise, over 30 s, to the stirred solution of HAIm and triethylamine, causing the precipitation of the target framework. This mixture was capped and placed at 60°C for 3 hours, and the product was isolated by filtration and suspended in 20 ml of methanol. This suspension was kept at 60°C overnight, and the product was again filtered and stirred in chloroform for 3 hours to remove any residual DMF. Lastly, the framework was isolated by filtration and evacuated at 80°C under vacuum overnight.

*Synthesis of SOD-Co(AIm)$_2$.*

**Mechanochemical synthesis:** The framework SOD-Co(**AIm**)$_2$ was obtained mechanochemically by ball-milling 0.25 mmol of cobalt(II) carbonate, 0.6 mmol of H**AIm**, and 25 μl of ethanol in a 15-ml stainless steel milling jar, using two stainless steel milling balls 7 mm in diameter (mass, 1.34 g each). The reaction mixture was milled for 60 min at a milling frequency of 30 Hz. After the preliminary PXRD analysis, the product was washed overnight with 15 ml of methanol, filtered, and evacuated overnight under vacuum at 80°C.

**Solution synthesis:** A mixture of 1 mmol of H**AIm** and 1 mmol of triethylamine was added to 15 ml of DMF and stirred at room temperature. A solution of 0.25 mmol of cobalt(II) nitrate hexahydrate in 20 ml of DMF was added dropwise to the ligand solution over a 10-min period, causing the precipitation of the deep-purple target framework. This mixture was allowed to stir for an additional 10 min, and then the solid was isolated by filtration and rinsed with acetone. After stirring overnight in 20 ml of chloroform, the product was again isolated by filtration, rinsed with acetone, and placed under vacuum at 80°C overnight, affording the activated final product (isolated yield, 82%).

*Synthesis of SOD-Cd(AIm)$_2$.*

**Mechanochemical synthesis:** The framework SOD-Cd(**AIm**)$_2$ was obtained mechanochemically using the ILAG methodology (*26*) by ball-milling 0.5 mmol of cadmium(II) oxide, 1.5 mmol of H**AIm,** 5 mg of $(NH_4)_2SO_4$ as the catalytic additive, and 100 μl of methanol as the milling liquid in a 15-ml stainless steel milling jar, using two stainless steel milling balls 7 mm in diameter (mass, 1.34 g). The mixture was milled for 70 min at a frequency of 30 Hz. After the PXRD analysis, the product was washed overnight with methanol and evacuated overnight under vacuum at 80°C.

**Solution synthesis:** A mixture of 1 mmol of H**AIm** and 1 mmol of triethylamine was added to 15 ml of DMF and stirred at room temperature. A solution of 0.25 mmol of cadmium(II) nitrate tetrahydrate in 20 ml of DMF was added dropwise to the ligand solution over a 10-min period, causing the precipitation of the target framework. The mixture was allowed to stir for an additional 10 min, and then the solid was isolated by filtration and rinsed with acetone. After stirring overnight in 20 ml of chloroform, the product was again isolated by filtration, rinsed with acetone, and placed under vacuum at 80°C overnight, affording the activated final product (isolated yield: 65%).

*Synthesis of SOD-Zn(VIm)$_2$.*

The framework SOD-Zn(**VIm**)$_2$ was obtained using the ILAG methodology (*26*) by milling of 1 mmol of zinc(II) oxide with a slight excess of 2.1 mmol of H**VIm** in the presence of 0.12 mmol of ammonium acetate as the catalytic salt additive and 100 μl of ethanol as the milling liquid (absolute, kept over molecular sieves), in a 15-ml stainless steel milling jar using two stainless steel milling balls 7 mm in diameter (mass, 1.34 g each). The mixture was milled for 30 min at a frequency of 30 Hz. After the PXRD analysis, the product was stirred overnight with 15 ml of methanol, filtered, and evacuated overnight under vacuum at 80°C. Alternative syntheses of this material have been reported (*28*, *46*).

*Synthesis of SOD-Co(VIm)$_2$.*

**Mechanochemical synthesis:** The framework SOD-Co(**VIm**)$_2$ was obtained mechanochemically by ball-milling 0.5 mmol of cobalt(II) carbonate, 1.2 mmol of H**VIm**, and 50 μl of ethanol in a 15-ml stainless steel milling jar, using two stainless steel milling balls 7 mm in

diameter (mass, 1.34 g each). The mixture was milled for 60 min at a frequency of 30 Hz. After the PXRD analysis, the product was washed overnight with 15 ml of methanol, filtered, and evacuated overnight under vacuum at 80°C.

**Solution synthesis:** The solution synthesis for SOD-Co(**VIm**)$_2$ was identical to that of SOD-Co(**AIm**)$_2$, replacing 1 mmol of H**AIm** with 1 mmol of H**VIm** (isolated yield, 32%).

*Synthesis SOD-Cd(VIm)$_2$.*

**Mechanochemical synthesis:** The framework SOD-Cd(**VIm**)$_2$ was obtained mechanochemically using the ILAG methodology (*26*) by ball-milling 0.5 mmol of Cd(OH)$_2$, 1.2 mmol of H**VIm**, 5 mg of ammonium methanesulfonate as the catalytic salt additive, and 75 μl of methanol in a 15-ml stainless steel milling jar, using two stainless steel milling balls 7 mm in diameter (mass, 1.34 g each). The mixture was milled for 25 min at a frequency of 30 Hz. After the preliminary PXRD analysis of the reaction mixture, the product was washed overnight with 15 ml of methanol and evacuated overnight under vacuum at 80°C.

**Solution synthesis:** The solution synthesis for SOD-Cd(**VIm**)$_2$ was identical to that of SOD-Cd(**AIm**)$_2$, replacing 1.1 mmol of H**AIm** with 1.1 mmol of H**VIm** (isolated yield, 30%).

## SUPPLEMENTARY MATERIALS

Supplementary material for this article is available at http://advances.sciencemag.org/cgi/content/full/5/4/eaav9044/DC1

Fig. S1. Reaction scheme for the synthesis of H**AIm**.
Fig. S2. NMR spectra for the ligand H**AIm**.
Fig. S3. Overlay of PXRD patterns of mechanochemically prepared ZIFs immediately after milling, compared to the simulated pattern for ZIF-8.
Fig. S4. Thermal analysis data for acetylene-substituted MOFs.
Fig. S5. Thermal analysis data for vinyl-substituted MOFs.
Fig. S6. Overlay of selected FTIR-ATR spectra.
Fig. S7. Selected solid-state NMR spectra.
Fig. S8. Comparison of PXRD patterns for selected MOFs after impact testing.
Fig. S9. Selected images of hypergolic drop tests on hypergolic ZIFs using RFNA oxidizer.
Fig. S10. Nitrogen desorption and adsorption curves for selected MOFs.
Fig. S11. Thermogravimetric analysis of ZIFs with included nitromethane guest.
Fig. S12. Selected examples of hypergolic drop tests on ZIFs containing guests.
Fig. S13. Calculated DOS plots for the herein studied frameworks.
Fig. S14. The hypergolicity of selected ZIFs after 1 month using WFNA as an oxidizer.
Fig. S15. Illustration of vinyl-substituent disorder in the structure of SOD-Co(**VIm**)$_2$.
Table S1. Summary of crystallographic and Rietveld refinement parameters.
Table S2. Reaction equations used in the calculation of combustion energies.
Table S3. Calculated bandgaps for herein studied ZIF structures.
Data file S1. Crystallographic data (in CIF format) for crystal structures of ZIF materials.
Data file S2. CheckCIF (in PDF format) for crystal structures of ZIF materials.
Data file S3. Movie (in MOV format) of an example drop test conducted using Co(**AIm**)$_2$, with WFNA as the oxidizer.

## REFERENCES AND NOTES


1. T. Brinck, Ed., *Green Energetic Materials*, (John Wiley & Sons, Ltd. 2014).
2. J. J. Sabatini, K. D. Oyler, Recent advances in the synthesis of high explosive materials. *Crystals* **6**, 5 (2016).
3. Y. Xu, Q. Wang, C. Shen, Q. Lin, P. Wang, M. Lu, A series of energetic metal pentazolate hydrates. *Nature* **549**, 78–81 (2017).
4. D. Trache, T. M. Klapötke, L. Maiz, M. Abd-Elghany, L. T. DeLuca, Recent advances in new oxidizers for solid rocket propulsion. *Green Chem.* **19**, 4711–4736 (2017).
5. M. Smiglak, A. Metlen, R. D. Rogers, The second evolution of ionic liquids: From solvents and separations to advanced materials energetic examples from the ionic liquid cookbook. *Acc. Chem. Res.* **40**, 1182–1192 (2007).
6. A. Mehrkesh, A. T. Karunanithi, Energetic ionic materials: How green are they? A comparative life cycle assessment study. *ACS Sustain. Chem. Eng.* **1**, 448–455 (2013).
7. J. C. Bennion, N. Chowdhury, J. W. Kampf, A. J. Matzger, Hydrogen peroxide solvates of 2,4,6,8,10,12-hexanitro-2,4,6,8,10,12-hexaazaisowurtzitane. *Angew. Chem. Int. Ed.* **55**, 13118–13121 (2016).
8. T. G. Witkowski, P. Richardson, B. Gabidullin, A. Hu, M. Murugesu, Synthesis and investigation of 2,3,5,6-tetra(1*H*-tetrazol-5-yl) pyrazine based energetic materials. *ChemPlusChem* **83**, 984–990 (2018).
9. D. Srinivas, L. A. Mitchell, D. A. Parrish, J. M. Shreeve, From FOX-7 to H-FOX to insensitive energetic materials with hypergolic properties. *Chem. Commun.* **52**, 7668–7671 (2016).
10. S. Schneider, T. Hawkins, M. Rosander, G. Vaghjiani, S. Chambreau, G. Drake, Ionic liquids as hypergolic fuels. *Energy Fuels* **22**, 2871–2872 (2008).
11. X. Zhang, L. Shen, Y. Luo, R. Jiang, H. Sun, J. Liu, T. Fang, H. Fan, Z. Liu, Synthesis and ignition properties research of 1,5-Diazabicyclo [3.1.0] hexane type compounds as potential green hypergolic propellants. *Ind. Eng. Chem. Res.* **56**, 2883–2888 (2017).
12. L. T. De Luca, T. Shimada, V. P. Sinditskii, M. Calabro, *Chemical Rocket Propulsion: A Comprehensive Survey of Energetic Materials* (Springer, 2016).
13. H. Tan, H. Terashima, M. Koshi, Y. Daimon, Hypergolic ignition and flame structures of hydrazine/nitrogen tetroxide co-flowing plane jets. *Proc. Combust. Inst.* **35**, 2199–2206 (2015).
14. P. D. McCrary, G. Chatel, S. A. Alaniz, O. A. Cojocaru, P. A. Beasley, L. A. Flores, S. P. Kelley, P. S. Barber, R. D. Rogers, Evaluating ionic liquids as hypergolic fuels: Exploring reactivity from molecular structure. *Energy Fuels* **28**, 3460–3473 (2014).
15. Q. Zhang, J. M. Shreeve, Energetic ionic liquids as explosives and propellant fuels: A new journey of ionic liquid chemistry. *Chem. Rev.* **114**, 10527–10574 (2014).
16. S. Li, H. Gao, J. M. Shreeve, Borohydride ionic liquids and borane/ionic-liquid solutions as hypergolic fuels with superior low ignition-delay times. *Angew. Chem. Int. Ed.* **53**, 2969–2972 (2014).
17. P. Silva, S. M. F. Vilela, J. P. C. Tomé, F. A. Almeida Paz, Multifunctional metal–organic frameworks: From academia to industrial applications. *Chem. Soc. Rev.* **44**, 6774–6803 (2015).
18. H. Furukawa, K. E. Cordova, M. O'Keeffe, O. M. Yaghi, The chemistry and applications of metal–organic frameworks. *Science* **341**, 1230444 (2013).
19. K. A. McDonald, S. Seth, A. J. Matzger, Coordination polymers with high energy density: An emerging class of explosives. *Cryst. Growth Des.* **15**, 5963–5972 (2015).
20. J. Zhang, Y. Du, K. Dong, H. Su, S. Zhang, S. Li, S. Pang, Taming dinitramide anions within an energetic metal–organic framework: A new strategy for synthesis and tunable properties of high energy materials. *Chem. Mater.* **28**, 1472–1480 (2016).
21. Y. Zhang, S. Zhang, L. Sun, Q. Yang, J. Han, Q. Wei, G. Xie, S. Chen, S. Gao, A solvent-free dense energetic metal–organic framework (EMOF): To improve stability and energetic performance via in situ microcalorimetry. *Chem. Commun.* **53**, 3034–3037 (2017).
22. S. Zhang, Q. Yang, X. Liu, X. Qu, Q. Wei, G. Xie, S. Chen, S. Gao, High-energy metal–organic frameworks (HE-MOFs): Synthesis, structure and energetic performance. *Coord. Chem. Rev.* **307**, 292–312 (2016).
23. L. H. Blair, A. Colakel, R. M. Vrcelj, I. Sinclair, S. J. Coles, Metal–organic fireworks: MOFs as integrated structural scaffolds for pyrotechnic materials. *Chem. Commun.* **51**, 12185–12188 (2015).
24. K. S. Park, Z. Ni, A. P. Côté, J. Y. Choi, R. Huang, F. J. Uribe-Romo, H. K. Chae, M. O'Keeffe, O. M. Yaghi, Exceptional chemical and thermal stability of zeolitic imidazolate frameworks. *Proc. Natl. Acad. Sci. U.S.A.* **103**, 10186–10191 (2006).
25. J.-P. Zhang, Y.-B. Zhang, J.-B. Lin, X.-M. Chen, Metal-azolate frameworks: From crystal engineering to functional materials. *Chem. Rev.* **112**, 1001–1033 (2012).
26. P. J. Beldon, L. Fábián, R. S. Stein, A. Thirumurugan, A. K. Cheetham, T. Friščić, Rapid room-temperature synthesis of zeolitic imidazolate frameworks by using mechanochemistry. *Angew. Chem. Int. Ed.* **49**, 9640–9643 (2010).
27. J. C. S. Remi, T. Rémy, V. Van Hunskerken, S. van de Perre, T. Duerinck, M. Maes, D. De Vos, E. Gobechiya, C. E. A. Kirschhock, G. V. Baron, J. F. M. Denayer, Biobutanol separation with the metal–organic framework ZIF-8. *ChemSusChem* **4**, 1074–1077 (2011).
28. J. M. Marrett, C. Mottillo, S. Girard, C. W. Nickels, J.-L. Do, G. Dayaker, L. S. Germann, R. E. Dinnebier, A. J. Howarth, O. K. Farha, T. Friščić, C.-J. Li, Supercritical carbon dioxide enables rapid, clean, and scalable conversion of a metal oxide into zeolitic metal–organic frameworks. *Cryst. Growth Des.* **18**, 3222–3228 (2018).
29. G. P. Rachiero, H. M. Titi, R. D. Rogers, Versatility and remarkable hypergolicity of *exo*-6, *exo*-9 imidazole-substituted *nido*-decaborane. *Chem. Commun.* **53**, 7736–7739 (2017).
30. A. C. Wright, *USAF Propellant Handbooks. Nitric Acid/Nitrogen Tetroxide Oxidizers. Volume II* (Martin Marietta Aerospace Denver CO, 1977).
31. S. Li, Y. Wang, C. Qi, X. Zhao, J. Zhang, S. Zhang, S. Pang, 3D Energetic metal-organic frameworks: Synthesis and properties of high-energy materials. *Angew. Chem. Int. Ed.* **52**, 14031–14035 (2013).
32. J. Zhang, H. Su, Y. Dong, P. Zhang, Y. Du, S. Li, M. Gozin, S. Pang, Synthesis of denser energetic metal-organic frameworks via a tandem anion-ligand exchange strategy. *Inorg. Chem.* **56**, 10281–10289 (2017).
33. W. Zhu, H. Xiao, First-principles band gap criterion for impact sensitivity of energetic crystals: A review. *Struct. Chem.* **21**, 657–665 (2010).

34. Z. Zheng, X. Jiang, J. Zhao, Structural, electronic and elastic properties of several metal organic frameworks as a new kind of energetic materials. *Chem. Phys. Lett.* **628**, 76–80 (2015).
35. S. J. Clark, M. D. Segall, C. J. Pickard, P. J. Hasnip, M. I. J. Probert, K. Refson, M. C. Payne, First principles methods using CASTEP. *Z. Kristallogr.* **220**, 567–570 (2005).
36. J. P. Perdew, K. Burke, M. Ernzerhof, Generalized gradient approximation made simple. *Phys. Rev. Lett.* **77**, 3865–3868 (1996).
37. S. Grimme, Semiempirical GGA-type density functional constructed with a long-range dispersion correction. *J. Comput. Chem.* **27**, 1787–1799 (2006).
38. D. L. Omellas, *Calorimetric Determination of the Heat and Products of Detonation for Explosives: October 1961 to April 1982* (UCRL-52821, Lawrence Livermore National Laboratory, 1982).
39. J. P. L. Perez, B. W. McMahon, S. L. Anderson, Functionalization and passivation of boron nanoparticles with a hypergolic ionic liquid. *J. Propuls. Power* **29**, 489–495 (2013).
40. K. A. McDonald, J. C. Bennion, A. K. Leone, A. J. Matzger, Rendering non-energetic microporous coordination polymers explosive. *Chem. Commun.* **52**, 10862–10865 (2016).
41. S. Seth, K. A. McDonald, A. J. Matzger, Metal effects on the sensitivity of isostructural metal–organic frameworks based on 5-amino-3-nitro-1*H*-1,2,4-triazole. *Inorg. Chem.* **56**, 10151–10154 (2017).
42. T. Björkman, CIF2Cell: Generating geometries for electronic structure programs. *Comput. Phys. Commun.* **182**, 1183–1186 (2011).
43. A. J. Morris, R. J. Nicholls, C. J. Pickard, J. R. Yates, OptaDOS: A tool for obtaining density of states, core-level and optical spectra from electronic structure codes. *Comput. Phys. Commun.* **185**, 1477–1485 (2014).
44. R. J. Nicholls, A. J. Morris, C. J. Pickard, J. R. Yates, OptaDOS—A new tool for EELS calculations. *J. Phys. Conf. Ser.* **371**, 012062 (2012).
45. O. Dirat, A. Clipson, J. M. Elliott, S. Garrett, A. B. Jones, M. Reader, D. Shaw, Regioselective synthesis of 4-(2-alkyl-5-methyl-2*H*-pyrazol-3-yl)-piperidines. *Tetrahedron Lett.* **47**, 1729–1731 (2006).
46. Q. Sun, H. He, W.-Y. Gao, B. Aguila, L. Wojtas, Z. Dai, J. Li, Y.-S. Chen, F.-S. Xiao, S. Ma, Imparting amphiphobicity on single-crystalline porous materials. *Nat. Commun.* **7**, 13300 (2016).



**Acknowledgments**

**Funding:** This research was supported by the Air Force Office of Scientific Research under AFOSR award no. FA9550-14-1-0306. This research was undertaken, in part, owing to funding from the Canada Excellence Research Chairs Program, the NSERC Discovery Grant (NSERC RGPIN-2017-06467), the NSERC E. W. R. Steacie Memorial Fund (NSERC SMFSU 507347-17), and the Canada CFI program. Computations were made on the supercomputer Mp2 from Université de Sherbrooke, managed by Calcul Québec and Compute Canada. The operation of this supercomputer was funded by the Canada Foundation for Innovation (CFI), the ministère de l'Économie, de la science et de l'innovation du Québec (MESI), and the Fonds de recherche du Québec–Nature et technologies (FRQ-NT). **Author contributions:** T.F. and R.D.R. organized and planned the research. H.M.T., J.M.M., G.D., G.P.R., and C.M conducted the experiments. M.A. conducted the theoretical calculations, with advice from A.J.M. **Competing interests:** T.F., R.D.R., H.M.T., J.M.M., M.A., and G.D. are inventors on a provisional patent application (serial no. 62/730,590, date 13 September 2018) related to this work assigned to ACSYNAM Inc. (Montreal, H1P 1W1, Canada) with T.F. and C.M. as cofounders and co-owners. All the other authors declare that they have no competing interests. **Data and materials availability:** All data needed to evaluate the conclusions in the paper are present in the paper and/or the Supplementary Materials. Additional data related to this paper may be requested from the authors. Crystal structures for Zn(**Alm**)$_2$, Co(**Alm**)$_2$, Cd(**Alm**)$_2$, Co(**Vlm**)$_2$, and Cd(**Vlm**)$_2$ are provided as data file S1 and are also deposited with the Cambridge Structural Database under deposition codes 1871958 to 1871962.

Submitted 2 November 2018
Accepted 13 February 2019
Published 5 April 2019
10.1126/sciadv.aav9044

**Citation:** H. M. Titi, J. M. Marrett, G. Dayaker, M. Arhangelskis, C. Mottillo, A. J. Morris, G. P. Rachiero, T. Friščić, R. D. Rogers, Hypergolic zeolitic imidazolate frameworks (ZIFs) as next-generation solid fuels: Unlocking the latent energetic behavior of ZIFs. *Sci. Adv.* **5**, eaav9044 (2019).

Science Advances

# Hypergolic zeolitic imidazolate frameworks (ZIFs) as next-generation solid fuels: Unlocking the latent energetic behavior of ZIFs

H. M. Titi, J. M. Marrett, G. Dayaker, M. Arhangelskis, C. Mottillo, A. J. Morris, G. P. Rachiero, T. Friscic and R. D. Rogers

*Sci Adv* **5** (4), eaav9044.
DOI: 10.1126/sciadv.aav9044